Science of the Total Environment 942 (2024) 173808

Contents lists available at ScienceDirect

Science of the Total Environment

journal homepage: www.elsevier.com/locate/scitotenv

Spatial distribution of small microplastics in the Norwegian Coastal Current

Fangzhu Wu [a,*], Lina Reding [a], Marrit Starkenburg [a], Clara Leistenschneider [a,b], Sebastian Primpke [a], Alvise Vianello [c], Karin A.F. Zonneveld [d,e], Mats B.O. Huserbråten [f], Gerard J.M. Versteegh [d,g], Gunnar Gerdts [a]

[a] Shelf Sea System Ecology, Alfred Wegener Institute Helmholtz Center for Polar and Marine Research, Kurpromenade 201, 27498 Helgoland, Germany
[b] Man-Society-Environment Program, Department of Environmental Sciences, University of Basel, 4051 Basel, Switzerland
[c] Department of the Built Environment, Aalborg University, 9220 Aalborg Øst, Denmark
[d] MARUM – Centre for Marine Environmental Sciences, University of Bremen, 28359 Bremen, Germany
[e] Department of Geosciences, University of Bremen, 28359 Bremen, Germany
[f] Department of Oceanography and Climate, Institute of Marine Research, 5817 Bergen, Norway
[g] Department of Physics and Earth Sciences, Constructor University, 28759 Bremen, Germany

HIGHLIGHTS

- Study on small microplastics in various depths of Norwegian Coastal Current waters
- Concentrations of small microplastics varied, notably higher in surface seawater.
- No notable geographical pattern in small microplastic concentrations (<4 m) in NCC
- Lagrangian model used to assess microplastic transport from Europe to the Arctic
- Introduction of new surface water sampler and assessment of ship's contamination

GRAPHICAL ABSTRACT

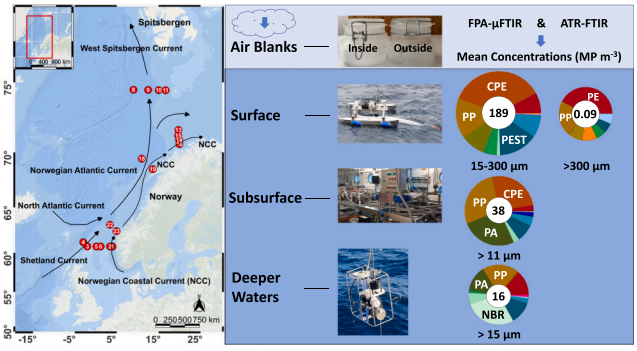

ARTICLE INFO

Editor: Kevin V. Thomas

Keywords:
Norwegian Coastal Current (NCC)
Microplastics (MPs)
Lateral and vertical distribution
FTIR microscopy and spectroscopy
Lagrangian particle dispersal simulation

ABSTRACT

High concentrations of microplastic (MP) particles have been reported in the Arctic Ocean. However, studies on the high-resolution lateral and vertical transport of MPs from the European waters to the Arctic are still scarce. Here, we provide information about the concentrations and compositions of MPs in surface, subsurface, and deeper waters (< 1 m, ~ 4 m, and 17–1679 m) collected at 18 stations on six transects along the Norwegian Coastal Current (NCC) using an improved Neuston Catamaran, the COntinuos MicroPlastic Automatic Sampling System (COMPASS), and in situ pumps, respectively. FTIR microscopy and spectroscopy were applied to measure MP concentration, polymer composition, and size distribution. Results indicate that the concentrations of small microplastics (SMPs, <300 μm) varied considerably (0–1240 MP m^{-3}) within the water column, with significantly higher concentrations in the surface (189 MP m^{-3}) and subsurface (38 MP m^{-3}) waters compared to deeper waters (16 MP m^{-3}). Furthermore, the average concentration of SMPs in surface water samples was four orders of magnitude higher than the abundance of large microplastics (LMPs, >300 μm), and overall, SMPs <50 μm account for >80 % of all detected MPs. However, no statistically significant geographical patterns were

* Corresponding author.
E-mail address: fangzhu.wu@awi.de (F. Wu).

https://doi.org/10.1016/j.scitotenv.2024.173808
Received 31 January 2024; Received in revised form 3 June 2024; Accepted 4 June 2024
Available online 5 June 2024

observed in SMP concentrations in surface/subsurface seawaters between the six sampling transects, suggesting a relatively homogeneous horizontal distribution of SMPs in the upper ocean within the NCC/Norwegian Atlantic Current (NwAC) interface. The Lagrangian particle dispersal simulation model further enabled us to assess the large-scale transport of MPs from the Northern European waters to the Arctic.

1. Introduction

Microplastics (MPs, <5 mm (Arthur et al., 2009)) have globally infiltrated marine ecosystems, including remote polar regions (Bergmann et al., 2022; Leistenschneider et al., 2021; Suaria et al., 2020). Contamination spans various Arctic environmental components: surface and subsurface seawaters, water column, deep-sea sediments, sea ice, Arctic snow, and marine biota (Bergmann et al., 2019; Lusher et al., 2015; Peeken et al., 2018; Teichert et al., 2021; Tekman et al., 2020). It is estimated that approximately 100–1200 t of plastic float in the ice-free waters of the Arctic Ocean (Cózar et al., 2017), and high-resolution circulation models suggest that ocean currents carry the plastic litter from the North Atlantic to these areas, where it then accumulates (Huserbraten et al., 2022).

One of the important potential transport routes for MPs into the Arctic Ocean is via the Norwegian Coastal Current (NCC), which connects populated areas of northern Europe to the Barents Sea (Cózar et al., 2017). The NCC consists of multiple water sources that continue to mix with other water bodies along a northward trajectory into the Arctic Ocean (Skagseth et al., 2011). One of the main water sources of the NCC is the inflow of Atlantic water with the Norwegian Atlantic Current (NwAC), which enters the Nordic Seas between Shetland and the Faroe Islands (Winther and Johannessen, 2006) and flows alongside the NCC. Other notable water masses mixing into the NCC on route to the Arctic include the Baltic Sea outflow and freshwater input from all the Northern European continental rivers (Kristiansen and Aas, 2015). Understanding the distribution of MPs within this array of water masses is crucial for comprehending the flow dynamics of MPs into the European Arctic.

Since the concept of MPs was first introduced (Thompson et al., 2004), most environmental investigations of marine MP pollution have focused on surface seawaters (Cózar et al., 2014; Maes et al., 2017; Song et al., 2014) and sediments (Bergmann et al., 2017; Maes et al., 2017; Mani et al., 2019). The seabed is the largest known reservoir for plastic debris (Li et al., 2023) and high quantities of MPs have been observed in deep-sea sediments (Bergmann et al., 2017; Tekman et al., 2020). Earlier studies suggested that the abundance of MPs in the surface ocean is much smaller than expected (Cózar et al., 2014; Eriksen et al., 2014). Recently, samples of large water volumes collected with pumps (Tekman et al., 2020; Zhao et al., 2022) or Niskin bottles (Kanhai et al., 2018) have revealed that MPs are also prevalent throughout the water column, suggesting that the marine water column could potentially be a vast reservoir for MPs. Therefore, studying the vertical distribution of MPs along the water column is of paramount importance to better understand their flux to the seafloor.

MPs have been reported in surface and subsurface (6 m depth) waters along the NCC from Tromsø to the southwest of Svalbard (Lusher et al., 2015), Norway, and throughout the water column in the Fram Strait (Tekman et al., 2020). Nevertheless, studies on the high-resolution lateral and vertical distribution of MPs from European waters to the Arctic remain scarce. To detect potential MP concentration gradients from densely populated European coastal areas to relatively sparsely populated Norwegian coastal areas, and to realistically assess the overall migration of MPs to the Arctic Ocean through modelling, fine-scale quantification of MPs from multiple sources is required. This study represents the first assessment of MP distribution in surface, subsurface, and deeper Norwegian waters, providing a comprehensive overview of MP concentrations, polymer compositions, and size distributions. Using a Lagrangian particle dispersal simulation model, we further assessed the pathways of MP transport from northern European waters to the Arctic.

2. Materials and methods

2.1. Study area

Samples were collected on board the research vessel (RV) *Heincke* (He578, 4th June-7th July 2021) from six transects in Norwegian coastal waters (Fig. 1A, 18 stations, details see Table S1, Supporting Information (SI)). These transects were selected based on the results of an oceanographic model highlighting where different water masses intersect, including the NCC, Atlantic water, and Arctic water (Fig. S1). Samples were categorized based on their depths into surface, subsurface, and deeper waters (<1 m, ~4 m, and 17–1679 m). Sampling started from several coastal and offshore stations in Norway (Fedje Shetland transect) and from there through the Shetland Channel up to the northernmost sampling point (Latitude 74.50°N), in an area near Bjørnøya (Bear Island).

2.2. Water samples collection

At each station, oceanographic parameters were recorded by a CTD/Rosette probe (Seabird, USA) before any other sampling activity to identify different water masses based on their related physical features such as salinity, water temperature, and turbidity (Fig. S2, Table S1). All samples were stored at −20 °C until further analysis.

2.2.1. Surface water sampling

In total, 32 surface water samples (large microplastics, LMPs, 300–5000 μm, $n = 14$; small microplastics, SMPs, <300 μm (Enders et al., 2015; Gunaalan et al., 2023a; Gunaalan et al., 2023b), $n = 18$, (AMAP, 2021)) were collected utilizing an improved Neuston Catamaran (Fig. S3, AWI Helgoland, Germany). The device allows simultaneous sampling of LMPs and SMPs for the first time. It was towed alongside the vessel for 25–30 min at an average speed of 3.7 km/h with a lateral distance of ~5 m from the hull. The device was equipped with a Neuston net (mesh size, 300 μm; rectangular aperture 30 × 15 cm^2; Hydro-Bios Apparatebau GmbH, Germany) and a pumping and filtration system (see Fig. S3). The Neuston net was used to collect LMPs, with only half of the net opening immersed in water due to the floats. A mechanical flowmeter (Hydrobios, Germany) was attached to the net opening to calculate the volume of water filtered, which averaged 26.4 (± 6.0 S.D.) m^3 per sample (Table S1). Meanwhile, SMPs were first filtered through a stainless steel intake cartridge filter (Fig. S3, mesh size, 300 μm, Wolftechnik, Germany) and then collected on a stainless steel 15 μm filter mesh (Ø 293 mm; GKD, Germany) using a polytetrafluoroethylene (PTFE) membrane pump (E-Serie, Typ E 15 T T T; Almatec, Germany) driven by compressed air (Bauer, Germany) stored in two scuba tanks (15 L, 232 bar, Eurocylinder Systems AG, Germany). A water smart flowmeter (Gardena, Germany) was used to record the volume of filtered water, with an average volume of 0.5 (± 0.1 S.D.) m^3 per sample (Table S1). The Catamaran was only deployed under calm weather conditions; otherwise, a sampling Buoy (Fig. S3) with the same operation principle was applied to collect SMPs. After trawling, the net was carefully removed and rinsed off on the deck from the outside with a hose. Additionally, the net was rinsed with filtered (mesh size: 0.5 μm) freshwater stored in a high-performance sprayer (510 T, Gloria, Germany). Subsequently, the cod-end was detached, placed into a stainless-

steel bucket, and carefully rinsed from the outside with pre-filtered (0.2 μm) ethanol (EtOH, 99.5 %, Carl Roth, Germany). Afterwards, the contents of the cod-end sampler were transferred to a 2.5 L glass jar vial filled to a volume of ~1.25 L with EtOH to preserve the sample. Meanwhile, the filter holder lid was opened, and the sampling filter was carefully folded in half 3 times and transferred to a 1.5 L glass jar. After each sampling, the stainless steel cartridge filter was flushed thoroughly with freshwater on deck and then rinsed with filtered freshwater (mesh size: 0.5 μm), but not examined for potential SMP blockage, potentially leading to SMP underestimation.

2.2.2. Subsurface water sampling

A total of 13 subsurface water samples were successfully collected using the COntinuos MicroPlastic Automatic Sampling System (COMPASS) designed by Aalborg University, Denmark (Fig. 1A, except for Stations S13–15, S18 and S22). The system drew water using a submersible pump (Grundfos Unilift, Denmark) from the saltwater intake located 4 m below the Moon Pool of the RV *Heincke*. The water was transported to the wet lab through steel pipes and hoses, dimmed by a second plastic-free pump (Oberdorfer, Germany), and then entered a valve system distributing water to three plastic-free filtering devices (UFO system, Universal Filtering Objects system (Gunaalan et al., 2023a; Liu et al., 2023; Rist et al., 2020)). For this static sampling, only one of the three filtering systems was used. In brief, a single UFO system comprises three interconnected stainless-steel filtering units holding large diameter steel filters (Ø 167 mm; 1 × 300 μm and 2 × 10 μm): the water was pre-filtered down to 300 μm in the first unit and then filtered in parallel to 10 μm in the other units. The outflow was recombined, and the volume was measured with a mechanical water meter (Zenner, Germany), yielding an average filtered volume of 1.1 (± 0.2 S.D.) m^3 per sample (Table S1). After sampling, the three filters were carefully removed and placed in one pre-cleaned glass Petri dish and analysed together as a pooled sample for further MP extraction and identification.

2.2.3. Deeper waters sampling

To gain insights into the vertical transport of MPs in the deeper waters, two WTS-LV pumps (LV08, McLane Research Laboratories, USA) were tethered to a single wire at each station and deployed at predetermined depths for sampling. Two sampling depths (Table S1) were determined from CTD profiles, and only water below the deep chlorophyll maximum or pycnocline was sampled (Paragraph S1, Fig. S4). For each pump unit, seawater was pumped directly through a pre-cleaned 15 μm stainless steel filter mesh (Ø 142 mm, GKD, Germany). All pumps were programmed to run until 500 L of seawater had been filtered. After sampling, the filters were carefully transferred to pre-cleaned glass Petri dishes (Ø 18 mm) and sealed thoroughly with parafilm (Pechiney Plastic Packaging, U.S.A.). A total of 37 samples were successfully collected. Due to mechanical failure, six in situ pump samples (from S18, S19 and S22) were lost during MP extraction.

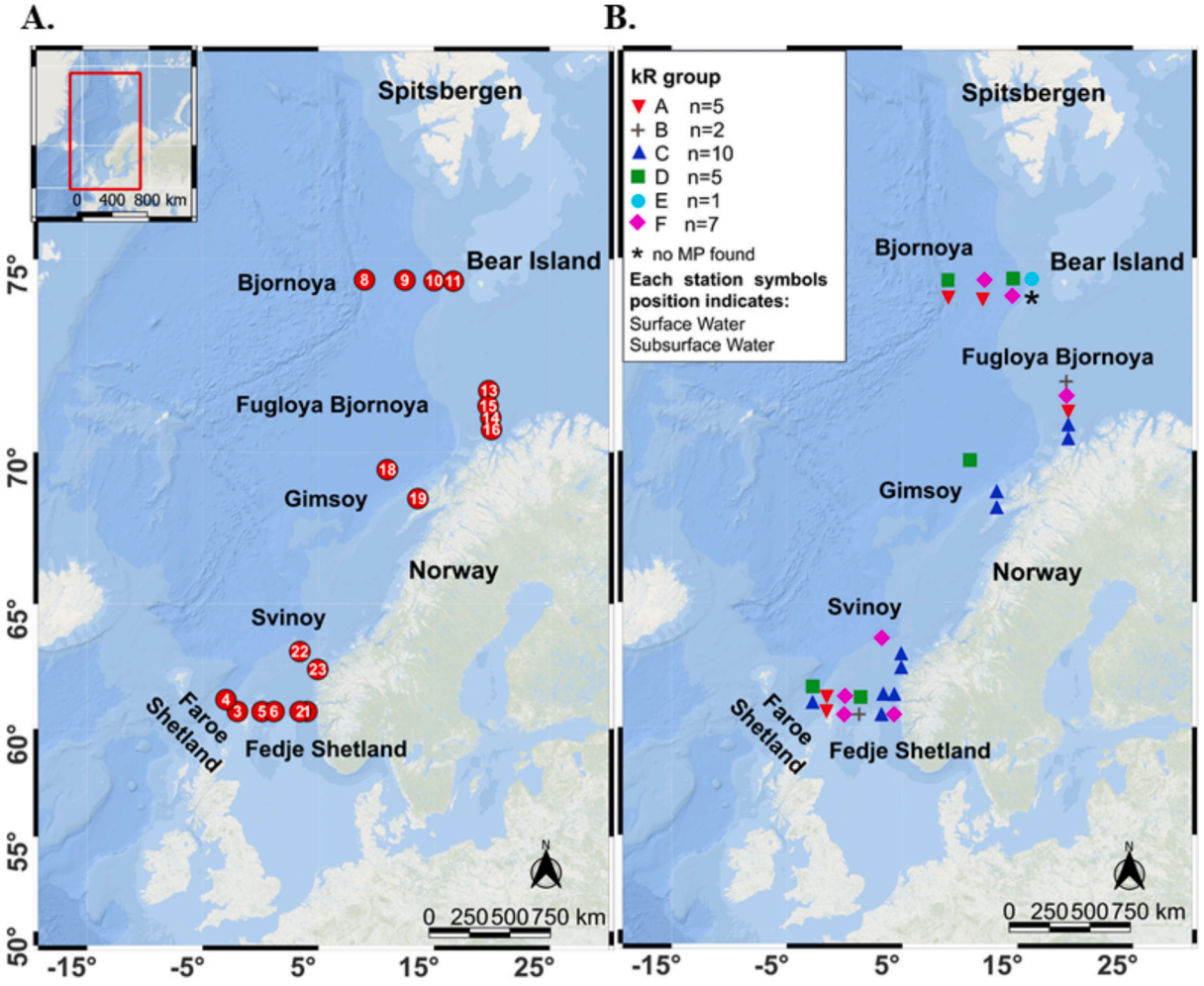

Fig. 1. (A) Map of the study area with the sampling sites and sampling transects. (B) Map of sampling area with 18 stations of surface water samples and 13 stations of subsurface samples and their assigned groups (different colours) based on kR-clustering. The maps were produced using QGIS with the base map ESRI ocean.

2.3. Microplastic extraction

2.3.1. Large microplastics

LMPs collected by Neuston net were visually inspected under a stereomicroscope (Olympus SZX16, Olympus, Germany). Samples were first transferred to a Bogorov counting chamber, and putative MP items were selected based on the following criteria (Zhao et al., 2018): (1) particles that were not easily broken by tweezers, (2) particles with uniform distribution of colour, and (3) particles without organic or cellular structures. The respective particles were then transferred to glass Petri dishes and photographed with a microscope camera (Olympus DP26 Digital Camera, Olympus) linked to the imaging software CellSens (Olympus, Germany). The major and minor dimensions of the putative MPs were measured following the method of Simon et al. (2018). Here, the major axis is defined as the longest continuous axis through the centre of the item, while the minor axis is the longest dimension perpendicular to the major axis (Roscher et al., 2021). Putative MPs were assigned to specific shape-related groups: fragments, films, foams, fibres (Ø < 50 μm) and lines/filaments (Ø > 50 μm) (Tanaka and Takada, 2016).

2.3.2. Small microplastics

All pump samples collected on the stainless steel filters were processed following a multi-step extraction protocol (for workflow details, please see Paragraph S2, Fig. S5). In brief, the procedure consisted of three main steps: 1) SDS (0.1 % sodium dodecyl sulphate, *w/v*, Carl Roth, Germany) incubation of the stainless-steel filters at 40 °C for 24 h to detach/loosen collected particles from the filter and transfer of the particulate onto small 15 μm stainless steel filters (Ø 47 mm; GKD, Germany). 2) Oxidation (Fenton's treatment; according to Al-Azzawi et al. (2020) with minor modifications) with iron sulfate ($FeSO_4$, 20 g/L, AppliChem GmbH, Germany) and hydrogen peroxide (H_2O_2, 30 %, Fa. Bernd Kraft GmbH, Germany) for 20 min to digest organic materials and followed by transfer of treated samples onto new 15 μm stainless steel filters. 3) density separation with pre-filtered sodium bromide (NaBr, Gruessing GmbH, Germany, density = 1.53–1.58 g cm^{-3} (Quinn et al., 2017)) to remove heavy inorganic materials and concentrate the samples onto another new small 15 μm filter mesh, then flushed with Milli-Q water (Milli-Q, IQ 7000, Millipore, France) to remove any potential NaBr residues. Subsequently, the filter was rinsed with Milli-Q water, and the material was retained in a glass neck bottle (100 mL) and stored at 4 °C for later analysis. Two surface (S5 and S11) and six subsurface (S1, S4, S5, S11, S16 and S19) water samples with excessive diatom content were subjected to a second density separation with lithium heteropolythungstate (LST fast float, density = 2.0 g cm^{-3}, Central Chemical Consulting Pty Ltd., Australia, details see Fig. S6, Paragraph S3). For MP identification, the sample material was concentrated on aluminium oxide filters (Ø 25 mm; 0.2 μm pore size; Anodisc, Whatman, UK). Depending on the residual material load in the processed samples, one to 20 Anodisc filters were prepared per sample (Table S1). Anodisc filters were then stored in glass Petri dishes (Ø 6 cm) and dried for at least 24 h in a desiccator (Sicco, Bohlender GmbH, Germany) before further analysis.

2.4. Microplastic identification

2.4.1. Large microplastics

Putative LMPs were identified individually using Attenuated Total Reflection Fourier Transform Infrared Spectroscopy (ATR-FTIR) (Tensor 27 spectrometer with a platinum ATR unit, Bruker Optik GmbH, Germany), see Roscher et al. (2021) for complete details. Briefly, selected items were placed on the diamond crystal, and three replicate spectra were recorded with a resolution of 4 cm^{-1} and 32 co-added scans (spectral range: 400–4000 cm^{-1}) and compared against our reference library (Primpke et al., 2018). Particles with a hit quality above 700 (out of 1000) were counted as safely identified. If the match ranged between 600 and 700, the spectra were validated or rejected based on expert assessment, as suggested by other studies (Kroon et al., 2018; Lorenz et al., 2019; Lusher et al., 2013). Measurements with hit qualities below 600 were defined as 'not identified'.

2.4.2. Small microplastics

Putative SMPs concentrated on the Anodisc filters were measured by a μFTIR-microscope (Hyperion 3000) connected to a Tensor 27 spectrometer (Bruker Optik GmbH, Germany) equipped with a 3.5× objective and a 64 × 64 focal plane array (FPA) detector with a pixel size of 11 μm (defining the lower detection limit). Although the mesh size of the filters technically sets the lower size limit during sample processing, smaller particles may still have been captured, enabling analysis of MPs between 11 and 15 μm. A spectral range of 1250–3600 cm^{-1} was used for measurements, with 32 co-added scans collected per field at a resolution of 8 cm^{-1} (Roscher et al., 2021). A grid of 20–26 measurement fields was applied to cover all particles in the filtration area. The IR spectra obtained were processed with OPUS 8.5 software, followed by automatic MPs identification and quantification by siMPle (Primpke et al., 2020) with a reference database designed by Primpke et al. (2018) and updated by Roscher et al. (2022). Final tabular data were obtained by running an image analysis in MPAPP (version 1.1.1) (Primpke et al., 2019) for the size of each MP particle and the specified polymer clusters. The image analysis through MPAPP was performed based on the spectral matching process of Primpke et al. (2017) using matching scores from a minimum of 600 to a maximum of 2000. The database is grouped into polymer types for material identification with individual minimum matching scores. In this study, the polymer types proposed by Lorenz et al. (2019) and Roscher et al. (2022) were applied for the reliable identification of the spectra to achieve comparable results to previous studies.

2.5. Quality assurance and quality control

Several steps have been introduced to reduce potential contamination. If not explicitly stated, all laboratory containers used were made of glass or stainless steel and were thoroughly air-blown (Airbrush compressor AF186, Wildanger Technik GmbH, Germany) and rinsed with Milli-Q water before use. All polymeric items that could not be replaced with alternative glass items (e.g., bottle caps, filter holders, tubes) were made of PTFE. All containers used for sampling were precleaned in a laboratory glassware washer (Miele Professional PG 8583 CD, Germany), rinsed with Milli-Q water, and then packed. Stainless steel filters used for sampling were soaked in the lab cleaner (edisonite super, Schülke & Mayr GmbH, Germany) for 24 h, flushed with Milli-Q water, air-blown and then packed in stainless steel containers or Petri dishes. During the cruise, used equipment was covered with aluminium foil to minimise air exposure. In addition, all equipment used for sampling was rinsed with filtered fresh water (0.5 μm) before each sample was taken. Blank controls were carried out at each station, both inside and outside the vessel, to give an overall idea of the potential air contamination on the ship. For each blank, 250 mL of Milli-Q water was added to a 0.5 L glass jar and the jar opening was kept open during the sampling event. The opening and closing times of the blanks were recorded (Table S2). The ship blanks were stored frozen at −20 °C. For analyses, the ship blanks were thawed, filtered directly onto Anodisc filters, and analysed under FPA-μFTIR as SMPs. Materials from tow ropes and ship paint from the RV *Heincke* were used as reference material for comparison (see Figs. S7 and S8). A dust box (DB1000, G4 prefiltration, HEPA-H14 final filtration, Q¼ 950 m^3 h^{-1}, Mocklinghoff Lufttechnik, Germany) was installed in each laboratory to filter airborne particles. All sample processing steps were performed on a laminar flow bench (ScanLaf Fortuna, 1800; LaboGene, Denmark), except for the addition of 97 % H_2SO_4 and Tween 20, which was performed in a fume hood for safety reasons. The 15 μm stainless steel filter meshes (Ø 47 mm) used for sample processing were rinsed with Milli-Q water, soaked,

and sonicated for 3 min (Bandelin Sonorex, Bandelin electronic GmbH & Co.KG, Germany) before a final rinse with Milli-Q water before use. Procedural blanks ($n = 3$–6) comprised of cleaned filter meshes brought aboard the cruise, were prepared and analysed in parallel with environmental samples. All solutions used were pre-filtered through glass microfiber filters (GF/F, Ø 47 mm, 0.7 μm pore size, VWR, Germany) except for 97 % H_2SO_4. Cotton lab coats were worn to reduce contamination from synthetic textiles. Nitrile gloves were worn during Fenton's reaction for safety at work. In addition, polyoxymethylene (POM) was subtracted from in situ pump samples due to systematic contamination from the WTS-LV pump head (Zhao et al., 2022). Furthermore, Rubber type 3 (RT3) was excluded from all water samples as the spectra might be miss-assigned from lipids (Witzig et al., 2020) (Paragraph S4, Fig. S9), and acrylamide was excluded due to low-quality matches.

2.6. Statistical analysis

Data from each sample on polymer type, size, and count were corrected for contamination by subtracting the procedural blanks (Table S3). All aliquots per sample were summed up for analysis. Based on MP numbers and sampling volumes, MP item concentrations [n (MP) m^{-3}] were estimated for both LMPs and SMPs. The MP counts of particles (hereby after referring to particle-like SMPs) and elongated particles (hereby after referring to fibre-like SMPs, aspect ratio of 3:1 or higher (Primpke et al., 2019) were combined for data analysis. MP concentrations and polymer compositions in deeper waters of each station were calculated by averaging data from both upper and lower depths. The ship blanks data (Paragraph S5, Figs. S10 and S11) was not used to correct the MPs in all water samples as it was based on the glass jar exposure time and the size of the jar opening, whereas for all water samples, the filters were stored immediately after sampling. Percentages of polymer types were square root transformed (multivariate statistics) (Sokal and Rohlf, 1995). The multivariate analyses were carried out based on Hellinger distance transformation, a recommended measure for ordination and clustering of polymer species abundance data, which does not put high weights on rare (polymer) species (Legendre and Gallagher, 2001; Lorenz et al., 2019; Rao, 1995). To assess the polymer diversity, species richness was calculated. To test if samples from surface, subsurface, and deeper waters differed significantly in their polymer composition, followed by Pairwise Tests, permutational multivariate analysis (PERMANOVA) with 9999 permutations at a significance level $p < 0.05$ was applied. To visualize these differences, cluster analysis and canonical analysis on the principle coordinates (CAP) were carried out in PRIMER with PERMANOVA+ (PRIMER-E version 7). Kruskal-Wallis Test was carried out in STATISTICA (StatSoft) to test if MP concentrations differ significantly in different water layers and to show which polymer type had the greatest influence on observed differences. To identify how stations of surface and subsurface waters group individually in terms of polymer composition, a non-hierarchical clustering analysis was conducted using the k-means algorithm, coupled with a similarity profile test (SIMPROF, hereafter referred to as kR-clustering). This analysis was performed in PRIMER-7, utilizing the Hellinger distance matrix with data that had undergone square root transformation, excluding values of 0. The significance level for SIMPROF was set to 5 % and performed with 999 permutations to define the optimal number of k-groups (between 2 and 10) to describe the clustering of the samples, which is based on maximizing R. Maps showing the geographical position of the samples along with the MP concentrations and polymer compositions as well as the assigned kR-clustering groups were produced using QGIS 3.26.3 with the base map ESRI Ocean (QGIS Development Team). The salinity and temperature profile and graphs were created in SigmaPlot 13.0 (Systat Software Inc., USA).

2.7. Lagrangian ocean modelling

To quantify and visualize the drift potential of particles sampled during the cruise, a particle tracking algorithm coupled to a dynamical ocean model was employed. The hydrodynamic model used to represent the ocean currents in the study area was based on the Regional Ocean Modelling System (ROMS), a free-surface, hydrostatic, primitive equation ocean general circulation model (Shchepetkin and McWilliams, 2005). ROMS was run with a horizontal resolution of 4 × 4 km in an orthogonal, curvilinear grid covering parts of the North Atlantic, all the Nordic seas and the Barents Sea (see Lien et al. (2013) for details on model setup and, e.g. Lien et al. (2014) for model performance). To model the advection of particles in the horizontal plane, we applied the fourth-order Runge-Kutta scheme Lagrangian Advection and Diffusion Model (LADiM; (Ådlandsvik, 2022)) coupled with the velocity fields from ROMS. Here, 1000 particles were released from each of the 18 sampling stations on the day of sampling (June 4th - July 7th 2021), ten for every meter down to 100 m (in total 18.000 particles), and drifted for 20 days. Moreover, to get an overview of the potential source direction of the particles sampled we also ran a backwards integration of the particle tracking algorithm, running 20 days backwards in time using the same particle release scheme. Due to the generally unknown buoyancy of the sampled particles, the drift depth used was fixed, set at the onset of simulation (i.e. 0–100 m) but classified into three depth layers for visualization (0–20 m, 20–50 m, and 50–100 m).

3. Results

3.1. Distribution of microplastics

Overall, MPs (LMPs and SMPs) were detected in 93 % of all water samples collected, indicating that MPs are prevalent (0–1240 MP m^{-3}) throughout the water column in the NCC. The Kruskal-Wallis Test showed that the mean concentrations of SMPs in surface (189 MP m^{-3}, $p < 0.001$) and subsurface (38 MP m^{-3}, $p = 0.026$) seawaters were significantly higher than those in deeper waters (16 MP m^{-3}) (Fig. 2, Table S5). The Kruskal-Wallis Test results also revealed the polymer types contributing most to this dissimilarity (Table S5, polyvinyl chloride (PVC), $p < 0.001$; chlorinated polyethylene (CPE), polypropylene (PP), polyamide (PA), polyester (PEST), and acrylates/polyurethane (PUR)/varnish, $p < 0.01$; and polycaprolactone (PCL), $p < 0.05$).

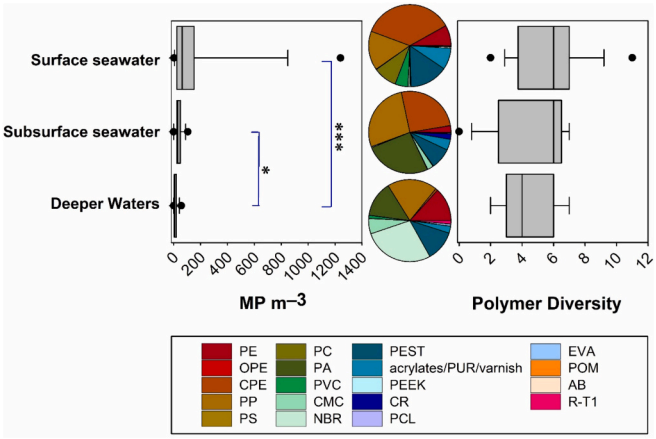

Fig. 2. Microplastic concentrations, polymer compositions, and polymer diversities in surface, subsurface, and deeper waters. Each boxplot indicates the median (central mark) and 25th and 75th percentiles, with whiskers outside the box indicating the 10th and 90th percentiles. Points outside the whiskers indicate outliers. (*$p = 0.026$, ***$p < 0.001$). PE: polyethylene, OPE: oxidized polyethylene, CPE: chlorinated polyethylene, PP: polypropylene, PS: polystyrene, PC: polycarbonate, PA: polyamide, PVC: polyvinyl chloride, CMC: chemically modified cellulose, NBR: nitrile rubber, PEST: polyester/polyethylene terephthalate, PUR: polyurethane, PEEK: polyether ether ketone, CR: polychloroprene, PCL: polycaprolactone, EVA: ethylene vinyl acetate, POM: polyoxymethylene, AB: acrylonitrile butadiene, R-T1: rubber type 1.

Notably, no statistically significant geographical patterns were observed in SMP concentrations in surface and subsurface seawaters between the six sampling transects (Table S6). The data showed a trend of decreasing polymer diversity (richness) with increasing sampling depths. Nevertheless, no notable variations were observed between surface, subsurface, and deeper waters, as illustrated in Fig. 2. The three investigated water layers (surface, subsurface, and deeper waters), differed greatly regarding polymer composition (PERMANOVA, Table S7, $p < 0.05$). The cluster analysis of surface and subsurface waters revealed that coastal stations formed a distinct group (group C, as shown in Fig. 1B), with CPE (52.2 %) having the highest proportion within this group, on average (Fig. 3). The separation of samples into different groups was also supported by CAP (details see Table S8), with a reasonably high correlation value of 0.906 and revealed two samples to be mismatched with a misclassification error of 6.667 % (Table S8).

3.1.1. Surface water samples

3.1.1.1. Neuston net samples. A total of 244 putative plastic items were visually sorted from 14 Neuston net samples, with 61.1 % ($n = 149$) of the selected particles displaying the same colour and characteristics as the coating of RV *Heincke* (Fig. S8). Subsequent ATR-FTIR spectroscopy confirmed that only 16.8 % ($n = 41$) of the selected particles were plastic, while 3.3 % were classified as natural polymers and 13.9 % were defined as 'not identified'. Additionally, 4.9 % of the presumed plastics were lost before measurement. Of the 41 plastic polymers detected in all 14 surface water samples, LMPs ($n = 33$) were present at 12 stations (Fig. S12), mesoplastics ($n = 7$, 5–25 mm, Fig. S13) and macroplastics (n = 1, >25 mm, Fig. S13) were present at four stations and one station, respectively. The concentrations of LMPs ranged from 0 (S1 and S3, Fig. 1A) to 0.45 (S14) MP m^{-3} with a mean of 0.09 (±0.11 S.D.) MP m^{-3}. Of all the LMPs detected, polyethylene (PE, 42.4 %) was the predominant polymer, followed by PP (21.2 %), polystyrene (PS, 9.1 %), and POM (9.1 %). PVC (6.1 %), PEST (6.1 %), and ethylene-vinyl acetate (EVA, 6.1 %) were also identified. PE was present in two (Svinoy and Fugloya Bjornoya) of the six sampled transects (Fig. 1A). Fragments (78.8 %) were the most common shape of LMPs, followed by foam (9.09 %), fibre (6.06 %), and filaments (6.06 %) (Fig. S14). The size ranged from 350 to 4236 μm, with the largest counts (30.3 %) observed in the 300–1000 μm size range (Fig. S15).

3.1.1.2. Catamaran & buoy samples. SMPs were detected in all 18 surface water samples with a mean quantity of 189 (±318 S.D.) MP m^{-3}. The highest number was at S1 (1240 MP m^{-3}), the easternmost station in the Fedje/Shetland transect, followed by S16 (805 MP m^{-3}), the southernmost station in the Fugloya Bjornoya transect, and S4 (410 MP m^{-3}), the westernmost station in the Faroe Shetland Channel transect (Fig. 1A). Eight stations had MP concentrations below 50 MP m^{-3}, with the lowest value at S11 (3 MP m^{-3}), the northernmost station in the Bjornya W transect (Fig. 1A, Fig. S12B, Table S1). Seventeen polymer types were identified by μFTIR imaging, with CPE being the predominant polymer (36.1 %, Fig. 2), particularly at coastal stations (S1, S2, S16, S19 and S23, Fig. 1A, Fig. S12B), accounting for 99.6 % of the CPE detected. The second highest polymer types were PP (15.4 %) and PEST (15.1 %), which were also the most widely distributed polymers, both detected at 16 stations (Fig. S12B, Table S1). Polymer diversity ranged from 2 to 11 different types (Fig. 2), with the lowest (S11) and highest (S1) diversity recorded at the sampling stations with the lowest and highest MP concentrations, respectively. Ten different polymer types

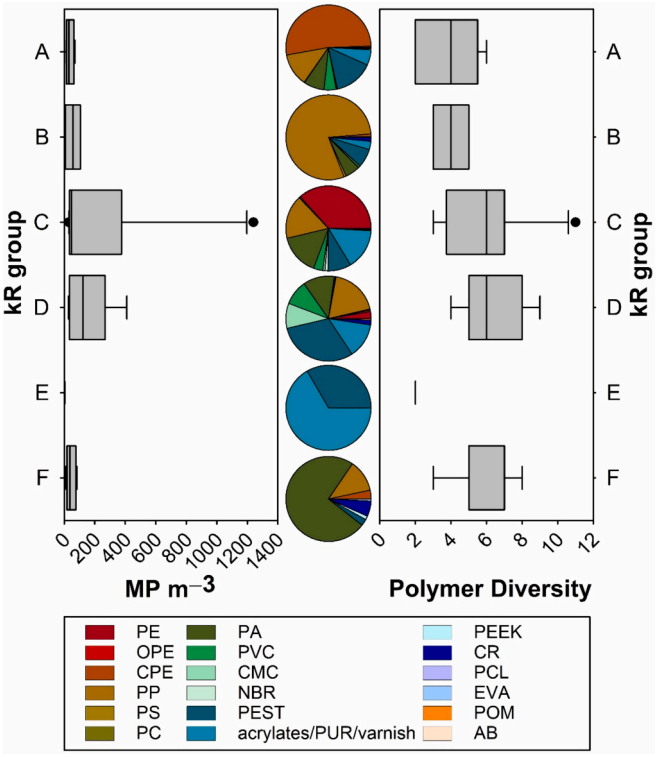

Fig. 3. Microplastic concentrations, polymer compositions, and polymer diversities of each kR group. Numbers of the stations of each kR group A: $n = 5$, B: $n = 2$, C: $n = 10$, D: n = 5, E: n = 1, F: $n = 7$. Each boxplot indicates the median (central mark) and 25th and 75th percentiles, with whiskers outside the box indicating the 10th and 90th percentiles. Points outside the whiskers indicate outliers. PE: polyethylene, OPE: oxidized polyethylene, CPE: chlorinated polyethylene, PP: polypropylene, PS: polystyrene, PC: polycarbonate, PA: polyamide, PVC: polyvinyl chloride, CMC: chemically modified cellulose, NBR: nitrile rubber, PEST: polyester/polyethylene terephthalate, PUR: polyurethane, PEEK: polyether ether ketone, CR: polychloroprene, PCL: polycaprolactone, EVA: ethylene vinyl acetate, POM: polyoxymethylene, AB: acrylonitrile butadiene.

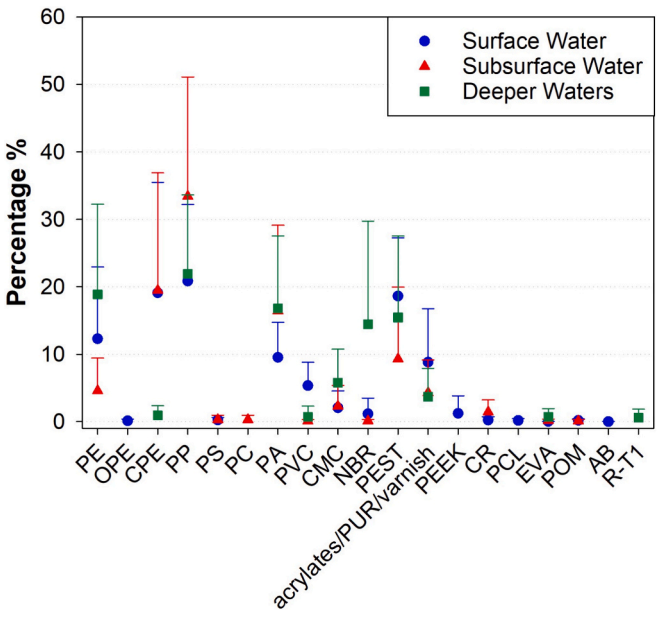

Fig. 4. Mean percentage of each polymer type in surface, subsurface and deeper waters. PE: polyethylene, OPE: oxidized polyethylene, CPE: chlorinated polyethylene, PP: polypropylene, PS: polystyrene, PC: polycarbonate, PA: polyamide, PVC: polyvinyl chloride, CMC: chemically modified cellulose, NBR: nitrile rubber, PEST: polyester/polyethylene terephthalate, PUR: polyurethane, PEEK: polyether ether ketone, CR: polychloroprene, PCL: polycaprolactone, EVA: ethylene vinyl acetate, POM: polyoxymethylene, AB: acrylonitrile butadiene, R-T1: rubber type 1. Whiskers show a 95 % confidence interval.

contribute, on average, between 1.2 % (nitrile rubber, NBR) and 20.8 % (PP) to the polymer composition, while seven polymer types contribute <1 % (in descending order): PS, polychloroprene (CR), POM, PCL, oxidized PE (OPE), EVA and acrylonitrile-butadiene (AB) (Fig. 4).

3.1.2. Subsurface water samples

MPs were found in 12 of the 13 (92.3 %) subsurface water samples (Fig. S12C). MP concentration ranged from 0 (S11) to 106 (S6) MP m^{-3} with an average of 38 (±26 S.D.) MP m^{-3} (Fig. 2). The only sample (S11) free from MPs was found closest to Bear Island, Norway (Fig. 1A). Fourteen polymer types were identified, of which PP (27.3 %) was the predominant polymer (Fig. 2) and the most widely distributed, being present at all stations where MPs were detected. Polymer diversity ranged from 0 to 7 types (Fig. 2), with stations S1, S2 and S10 having the highest polymer diversity (Fig. 1A). Eight polymer types contribute, on average, between 1.4 % (CR) and 33.4 % (PP) to the polymer composition, while six polymer types contribute <1 % (Fig. 4).

3.1.3. Deeper water samples

MPs were found in 28 of the 30 (93.3 %) deeper water samples. Two samples (upper water layer from S14 and lower water layer from S15) with no detectable MPs were both from the Fugloya Bjornoya transect (Fig. 1A). On average, MPs were found at all 15 stations sampled, with concentrations ranging from 1 (S16) to 58 (S10) MP m^{-3} with NBR (27.9 %) being the predominant polymer, followed by PP (19.6 %) and PA (14.0 %) (Fig. 2). Fig. 4 shows that seven polymer types contribute, on average, between 3.7 % (acrylates/PUR/varnish) and 21.9 % (PP) to the polymer composition, while four polymer types contribute <1 %.

3.2. Polymer shape and size distribution

In all water samples analysed by FPA-μFTIR, MPs were predominantly particles with a relative abundance of 83–87 %, while 13–17 % were elongated particles (Fig. S16). Concerning the size distribution, the most abundant particles were found in the size category 11 μm (58.2 %), whereas the most abundant elongated particles were in the 25–50 μm category (29.8 %) (Fig. 5). Similar trends were also identified in different water layers (surface, subsurface, and deeper waters) (Fig. S17).

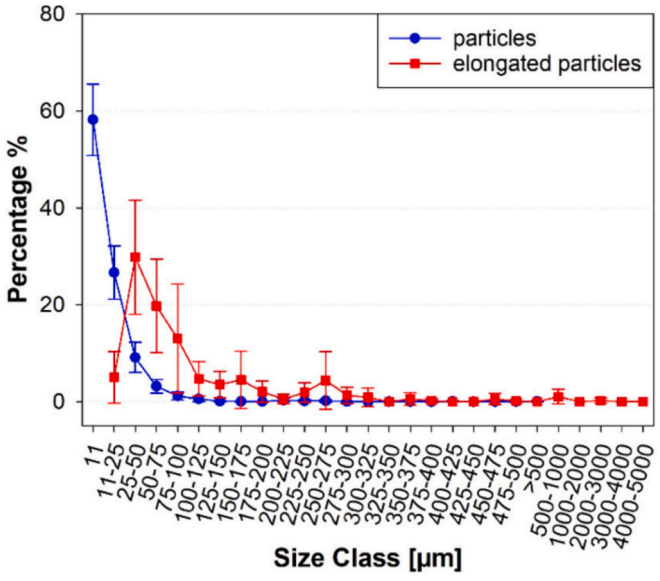

Fig. 5. Mean percentage of each size class in μm for particles and elongated particles in all water samples. Whiskers show a 95 % confidence interval.

3.3. Lagrangian circulation modelling

Based on the 20-day forward and backwards integration of the coupled ocean model/particle tracking algorithm, the surface interval (0–20 m) of the sampled water masses showed a significant northbound drift, especially along the continental slope shouldering the Norwegian Sea (Fig. 6). Specifically, there was a strong residual north-eastern drift from the northern station (S4) of the Faroe-Shetland channel transect; the first (near coastal) station (S23) of the Svinøy transect; the first (near coastal) station (S19) of the Gimsøy transect; all four stations of the Fugløya transect (S13-S16); and second station (S10) of the Bjørnøya transect (Fig. 6). There was a low residual drift around in the northern parts of the North Sea as well outshore of the continental slope (at least on the time scale of 20-d forward/backwards (+/−)). The general trend of high residual drift along the continental slope was also apparent in the deeper water masses, although not as pronounced - reflecting the slower flow of deeper water masses (Figs. S18–S19).

4. Discussion

4.1. Microplastic transport from south to north

Overall, MPs (LMPs and SMPs) were detected in 93 % of the samples collected from all water layers, indicating that MPs are widespread (at up to 1240 MP m^{-3}) throughout the water column in the NCC and the associated North Atlantic Waters of the NwAC flowing alongside it. Thus, it appears, that the NCC and NwAC together play an integral role in transporting MPs from Northern Europe into the Arctic. This was further verified with our modelling work that showed the general northwards flow of most of the sampled water masses across all depth layers, although with a lesser degree of northward drift at increasing depth. At the same time, our study showed no statistically significant geographical patterns in SMP concentrations in surface/subsurface seawater between the six sampling transects, indicating a relatively homogeneous horizontal distribution of SMPs in the upper ocean within the NCC/NwAC interface. These results support the hypothesis of

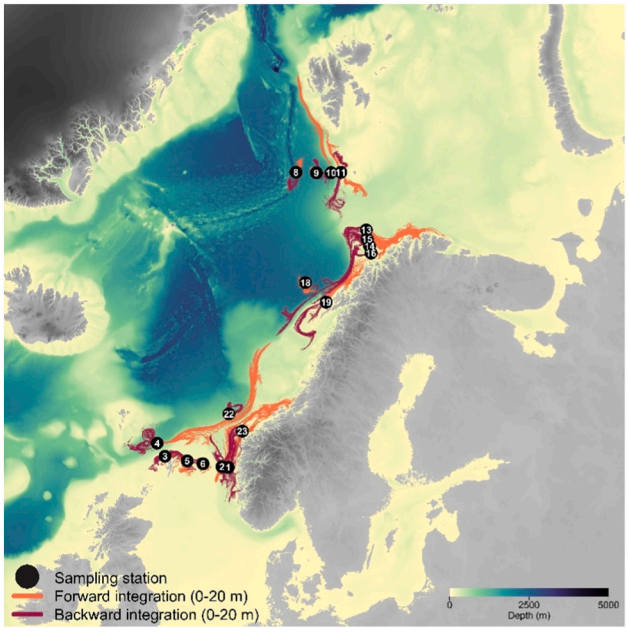

Fig. 6. Modelled horizontal transport of microplastics in the surface layer (0–20 m). Here orange lines represent the forward integration (20 d) of simulation from sampled sites (black circles), and purple lines represent the backward integration (−20 d). Elevation and bathymetric data were based on 'the GEBCO grid' (freely available at https:// www. gebco.net).

Huserbraten et al. (2022) within an extensive modelling framework, which showed that the Arctic Mediterranean may currently be in an advanced state of saturated accumulation of MPs, through a complex mechanism of transportation, accumulation, and re-circulation. Moreover, on average, the concentrations of SMPs (189 MP m^{-3}) in surface waters were four orders of magnitude higher than those of LMPs (0.09 MP m^{-3}), which is consistent with the few studies that were able to collect both pump and net samples (Rist et al., 2020; Zhao et al., 2022). In surface seawater, concentrations of SMPs at S1 (1240 MP m^{-3}) and S16 (805 MP m^{-3}) were comparingly high, which is unsurprising since they are both coastal stations sampling the core of the NCC, the main outflow of the highly polluted North Sea waters (e.g., see Karcher et al. (2012). However, the concentration of LMPs (0.09 MP m^{-3}) in surface seawater was one order of magnitude lower than in studies conducted in the Arctic (Lusher et al., 2015; Mu et al., 2019; Rist et al., 2020) and North Atlantic Ocean (Courtene-Jones et al., 2022) using similar sampling mesh sizes (300/333/335 μm). Possible explanations for these differences include variations in oceanographic features such as currents, direct windage, and wave-driven Stokes drift (Bergmann et al., 2022; Rist et al., 2020). The NCC, the NwAC, and the unstable interface between the two currents are known to be highly dynamic with respect to mesoscale structures (Isachsen, 2015; Mork and Blindheim, 2000; Wekerle et al., 2017), leading to considerable patchiness of positively buoyant matter at the surface (Haller, 2015). At the same time, as these results have been obtained from single expeditions, drawing definitive conclusions about the exact cause of this disparity remains challenging. In general, therefore, long-term monitoring and replicated studies are essential to provide good estimates of LMP concentrations in highly stochastic/patchy surface distributions.

Although the presence of MPs in deep-sea waters has been explored to some extent (Choy et al., 2019; Tekman et al., 2020; Uurasjarvi et al., 2021; Zhao et al., 2022), in-depth knowledge of the vertical distribution of MPs in the water column is still lacking. Several studies have reported higher concentrations of MPs in the pycnocline; for example, Choy et al. (2019) found MP concentrations were highest at intermediate depths into the mesopelagic zone (200–600 m). This could be explained by particles such as faecal pellets, planktons, minerals and MPs decelerating considerably in the sharp density gradients (Mrokowska, 2020). This decreases the sinking velocity of the particles, prolonging their residence time at density interfaces and potentially causing particle accumulation (Mrokowska, 2020; Zhao et al., 2022). Of all the deeper water samples collected in our study, only lower water layers from 8 stations (S4, S9–11, S13–15, S23, Table S1) were collected below the pycnocline, which defines the layer of rapid density change (Mrokowska, 2020). However, in contrast to previous reports stating that MPs preferably accumulate at stratified depth layers (Uurasjarvi et al., 2021), we find no statistical difference between concentrations of SMPs above (12 MP m^{-3}) and below (24 MP m^{-3}) the pycnocline (Table S1). The observed difference can be attributed to various factors. Unlike the previous studies that focused on MPs measuring 100 μm or larger, our research used two 15 μm meshes to collect samples from deeper waters and analysed particles down to 11 μm. Zhao et al. (2022) also noted a more uniform vertical distribution of SMPs (< 100 μm) in the South Atlantic Gyre, ascribing these results to SMPs' reduced susceptibility to stratification, slower settling speeds, and greater dispersion, enabling them to remain suspended in the water column for extended periods. Nevertheless, a further comparison with that study (Zhao et al., 2022) is hampered since their investigation excluded the first five meters of the water column, which were instead encompassed in our study. Noteworthy, our study found a significant difference in mean SMP concentration between deeper waters (16 MP m^{-3}) and surface (189 MP m^{-3}) and subsurface (38 MP m^{-3}) seawaters. These results align with D'Angelo et al. (2023), who reported elevated MP concentrations in the upper 50 m of the western Arctic seawater. This gradient across the water column is somehow expected. While surface seawaters in the NCC constantly receive plastic waste inputs from several sources (Bergmann et al., 2022), the complex sinking processes that drive SMPs to deeper waters (Kvale et al., 2020a; Zobkov et al., 2019) tend to create a dilution effect that becomes more evident with increasing depth. MPs' journey ends at the seafloor, a final reservoir where MPs accumulate over decades leading to high SMP concentrations also in the deep-sea sediments (Bergmann et al., 2017; Tekman et al., 2020). However, our results are derived from a single expedition, limiting our ability to assess temporal variations in MP distribution. Long-term MP monitoring in the NCC, coupled with higher-resolution ocean MP models, would significantly enhance our understanding of the complex mechanisms governing vertical MP transportation.

In terms of polymer composition, it is noteworthy that although there was a greater diversity of polymer types among SMPs ($n = 17$) in the surface seawaters compared to LMPs ($n = 7$), similarities in the predominant polymers were observed. Overall, PE (42.4 %) and PP (21.2 %) were the most common LMPs of the trawl samples, whereas SMPs were dominated by CPE (36.1 %) and PP (15.4 %), a pattern that has also been observed in the Arctic Ocean, North Sea, and the Atlantic Ocean (Hanninen et al., 2021; Zhao et al., 2022). In both size fractions, the highest polymer diversities were recorded at the sampling stations with the highest estimated MP concentrations (LMPs, polymer diversity = 4, S14 = 0.45 MP m^{-3}; SMPs, polymer diversity = 17, S1 = 1240 MP m^{-3}). In our study, the polymer diversity of SMPs tended to decrease with increasing depths but did not differ significantly. Both negatively and positively buoyant SMPs were identified throughout the water column. These findings are in agreement with Uurasjarvi et al. (2021), who suggested that the density of virgin plastic does not play a major role in the sinking rate of marine MPs as the density of the polymer could change due to bacterial biofilms and other biological processes (Kvale et al., 2020a; Kvale et al., 2020b). However, PERMANOVA analyses showed that the polymer composition differed significantly between surface, subsurface, and deeper waters. SMPs in the surface seawater were dominated by CPE, PP, and PEST in terms of polymer concentrations. In subsurface seawater, SMPs were mainly PP, PA, and CPE, with PP occurring at all stations where SMPs were detected. In contrast, NBR, PP, and PA were the dominant polymers in samples collected from deeper waters. However, when examining the average proportion of each polymer in each water compartment, it is evident that PP had the largest contribution in all water layers. Impressively, 99.6 % of the CPE in surface waters was detected at coastal stations (S1, S2, S23, S19 and S16), indicating that coastal input might be the main source of CPE. Such a pattern was also evidenced by cluster analysis of surface and subsurface waters, which revealed that these stations formed a distinct group, with CPE (52.2 %) having the highest proportion within this group, on average (Fig. 3). In addition, these stations are all located on the pathway of the NCC, so one may also assume that the NCC transported these particles from the same association. The prevalence of PP throughout the water column is not surprising since it is the most widely demanded plastic type in Europe (PlasticsEuope, 2022) and is extensively used for packaging, fishing gear, and other applications (PlasticsEurope, 2023). Its ubiquity has been widely documented in most environmental compartments (Bergmann et al., 2019; Cózar et al., 2014; Gunaalan et al., 2023a; Liu et al., 2018; O'Brien et al., 2023; Wang et al., 2021).

4.2. Small microplastics prevalent in the water column

The concentrations from the surface pump and the Neuston net samples differed by 3–4 orders of magnitude. This could be related to several factors. First, all pump samples were automatically identified and quantified by the FPA-μFTIR microscopy and image analysis, reducing the risk of losing particles compared to the visual-sort analysed net samples (Rist et al., 2020). Furthermore, large plastics tend to fragment into smaller pieces under various mechanisms (e.g. bio-, photo-, thermo-, thermo-oxidative degradation and hydrolysis (Andrady, 2011)), and it is expected that the size distribution of MPs

skews towards the smallest detectable size class (Mani et al., 2019). The SMP data from surface, subsurface, and deeper waters remarkably confirmed this principle. A similar trend was also reported by other studies using the same automatic FPA-μFTIR microscopy and size class categories, not only in seawater samples (Lorenz et al., 2019; Tekman et al., 2020) but also in other environmental matrices (e.g. sediment (Abel et al., 2021; Abel et al., 2022; Bergmann et al., 2017; Mani et al., 2019), sea ice cores (Peeken et al., 2018), and snow (Bergmann et al., 2019)). It is worth noting that in our study, the instrument has a lower detection limit of 11 μm. Based on the above-mentioned theory, we assume that MPs smaller than 11 μm, or nanoplastics, must be strikingly prevalent in the marine environment. However, limited by the current knowledge of sampling, sample extraction, and analytics, relevant field studies are sparse. From an ecological perspective, the majority of detected SMPs fall within the size range consumed by plankton-feeding marine invertebrates (Rist et al., 2020), overlapping with their natural prey. The ingestion of MPs between 7 and 150 μm has been already documented for different copepods (Cole et al., 2013; Sun et al., 2017; Vroom et al., 2017). This indicates that the potentially higher concentration of SMPs poses a greater risk to plankton feeders and other marine life due to an increased risk of penetration of biological barriers (Nel et al., 2009).

In our study, LMPs in the surface seawater were dominated by fragment-shaped MPs (78.8 %), which is consistent with the survey conducted along the NCC and the Baltic Sea (Hanninen et al., 2021). In contrast, Lusher et al. (2015) found that MPs detected from Tromsø, Norway, up southwest of the Svalbard archipelago were mainly fibres (95 %), and Ross et al. (2021) found the dominant role of fibres (92.3 %) in samples collected in the Arctic Ocean. These studies were carried out at higher latitudes than ours, and the authors suggested that fragmentation of larger plastic items such as fibres from maritime activities and long-distance transport by Atlantic waters and/or atmospheric inputs could explain the high amount of fibres in the eastern Arctic Ocean. The shape of fibres could reduce the drag and resistance as they move through the water compared to particles, allowing them more easily transported by ocean currents. Still, the hydrodynamic drag is also influenced by biofouling, buoyancy, size and density of the MPs, water turbulence and other environmental conditions, currently not allowing a clear explanation of these differences. In our study, it is truly remarkable that within the outdoor ship blanks, a substantial abundance of fibres was evident (Fig. S20), primarily recognized as natural cellulose through FPA-μFTIR analysis. Our results revealed a mere 20 % of the identified MPs in OSB were elongated particles. Notably, SMPs from surface, subsurface, and deeper waters were all predominantly particles (83–87 %) rather than elongated particles (13–17 %). Similar results were reported in the surface water samples from the Weser River and the North Sea (Roscher et al., 2021), surface water samples from Antarctica (Leistenschneider et al., 2024), surface and water column samples from the Kattegat/Skagerrak (Denmark) (Gunaalan et al., 2023a; Gunaalan et al., 2024), and water column samples from the Nuuk, west of Greenland, using comparable sampling and analytical methods (Rist et al., 2020).

4.3. Background air contamination on the ship

During the cruise, inside (ISB) and outside (OSB) ship blanks were collected during all sampling activities to help assess the background air contamination from the ship. The mean MP deposition rate in the ISB (582 MP h^{-1} m^{-2}) was higher than in the OSB (321 MP h^{-1} m^{-2}), but no significant differences were identified (Paragraph S5). Few studies have reported on the potential air contamination from the research vessel, and variations in ship blank sampling and analytical methods make it difficult to compare results across studies. However, our results provide informative data for future studies of air contamination from ships. According to the PERMANOVA analyses (Table S4), polymer compositions significantly differed between ISB and OSB. This can be explained by the fact that most sampling activities and equipment were on deck, which increased the sources of plastic in OSB as PEST (15 %), PA (14 %), PP (11 %), and acrylates/PUR/varnish (10 %) accounted for nearly 50 % of MPs detected. Notably, CPE was the predominant polymer in both inside (479 MP h^{-1} m^{-2}, 82.3 %) and outside (136 MP h^{-1} m^{-2}, 42.4 %) ship blanks (Fig. S10). Additionally, it was also the predominant polymer in surface seawater (36.1 %). Considering the concentration of MPs in OSB, we assume that atmospheric MPs or ship emissions may be a potentially large source of MPs in the open ocean and have been underestimated, but it could also be that MPs in the atmosphere were re-emitted from the ocean sea spray and bubble bursting (Allen et al., 2020; Gossmann et al., 2023). As stated in the methodology, these data were not used to correct MPs in all water samples due to sampling and calculation differences. They are only provided as background contamination data. However, this data is still a cautionary tale, and care needs to be taken to minimise the sample's exposure to air during the sampling, including air blanks when appropriate.

4.4. Comparison of sampling methods

Manta and Neuston nets have been used extensively to collect MPs from surface waters (Cózar et al., 2014; Eriksen et al., 2014) and have the main advantage of being able to sample large volumes of water fairly quickly. However, they are limited by mesh size, as 333/300 μm is considered a practical lower limit when sampling with nets. To capture MPs smaller than 500 μm, only very few studies have started to use filtration systems for surface water (< 1 m) sampling (Leistenschneider et al., 2024; Roscher et al., 2021). For example, Roscher et al. (2021) applied a custom-designed filtration system to sample MPs in the 11–500 μm size range in the German North Sea. Based on this design, we sampled surface seawaters using a newly developed Neuston Catamaran equipped with a Neuston net and a pump filtration system driven by compressed air (Fig. S3). This device allows the targeted and simultaneous sampling of LMPs and SMPs for the first time. This improvement facilitates a direct comparison between the characteristics of LMPs and SMPs at the same station, reducing the potential error compared to single Neuston net and pump sampling. In addition, the device offers significant time savings for offshore sampling as the samples can be collected in one haul. However, similar to most surface trawls, it can be limited by wave conditions when the sea state is rough. The cartridge filter and the net used (300 μm) can be replaced with smaller mesh sizes if desired in future studies. However, it's crucial to consider the potential for filter blockage to minimise particle loss. For subsurface seawater, we applied a COMPASS system, which operated simultaneously with the Neuston Catamaran to collect water at a depth of ~4 m. This novel sampling system allows filtering large volumes of water down to 10 μm independent from the sea state and weather conditions, providing yet an additional complementary sampling technique. It is activated and controlled from the wet lab, and can even be operated continuously and without supervision for several hours, allowing underway sampling (unpublished data).

5. Conclusion

This study provides a comprehensive data set on MPs' lateral and vertical distribution along the NCC from European waters to the Arctic. The concentrations and compositions of MPs in different water layers offer a unique snapshot of how MPs are distributed throughout the water column in the study area. Our findings highlight the prevalence of SMPs across the water column along the NCC and emphasize the predominant role of particles and the smallest size class (11 μm) SMPs. The absence of a discernible gradient in MP concentrations from south to north reinforces the significant role of the NCC in facilitating the transport of MPs from south to north. Additionally, the integration of results from a Lagrangian particle dispersal simulation model not only reaffirmed this transportation mechanism but also enabled us to evaluate the extensive-

scale conveyance of MPs from Northern European waters to the Arctic. Furthermore, we introduce the novel MP sampling equipment and evaluate the contribution of background contamination on the ship. This evaluation is crucial for establishing quality controls in MP research ensuring the reliability of research findings.

Funding

This work was supported under the framework of JPI Oceans by the German Federal Ministry of Education and Research (Project FACTS - Fluxes and Fate of Microplastics in Northern European Waters; BMBF grant 03F0849A) and Innovation Fund Denmark (Danmarks Innovationsfond - Project FACTS - Fluxes and Fate of Microplastics in Northern European Waters; 9087-00005B – FACTS). The work of S.P. was supported by funding from the European Union's Horizon 2020 Coordination and Support Action programme under Grant agreement 101003805 (EUROqCHARM). This output reflects only the author's view and the European Union cannot be held responsible for any use that may be made of the information contained therein. We thank the crew of RV *Heincke* for all their support during the cruise. We thank the workshop, AWI Helgoland, and Dr. Markus Brand from the Scientific Diving Centre, AWI Helgoland for technical support; We further thank Hannah Jebens, AWI Helgoland, for laboratory assistance, as well as Dr. Felix Weber, AWI Helgoland, for proofreading.

CRediT authorship contribution statement

Fangzhu Wu: Writing – review & editing, Writing – original draft, Visualization, Methodology, Investigation, Data curation. **Lina Reding:** Writing – review & editing, Visualization, Investigation. **Marrit Starkenburg:** Writing – review & editing, Visualization, Investigation. **Clara Leistenschneider:** Writing – review & editing, Methodology, Investigation. **Sebastian Primpke:** Writing – review & editing, Software, Resources, Data curation. **Alvise Vianello:** Writing – review & editing, Resources, Investigation. **Karin A.F. Zonneveld:** Writing – review & editing, Resources, Investigation. **Mats B.O. Huserbråten:** Writing – review & editing, Visualization, Software, Methodology. **Gerard J.M. Versteegh:** Writing – review & editing, Investigation. **Gunnar Gerdts:** Writing – review & editing, Supervision, Resources, Project administration, Investigation, Formal analysis.

Declaration of competing interest

The authors declare no competing financial interests or personal relationships that could have appeared to influence the work reported in this paper.

Data availability

I have already upload the research data as supplementary information

Appendix A. Supplementary data

Supplementary data to this article can be found online at https://doi.org/10.1016/j.scitotenv.2024.173808.

References

Abel, S.M., Primpke, S., Int-Veen, I., Brandt, A., Gerdts, G., 2021. Systematic identification of microplastics in abyssal and hadal sediments of the Kuril Kamchatka trench. Environ. Pollut. 269, 116095 https://doi.org/10.1016/j.envpol.2020.116095.

Abel, S.M., Primpke, S., Wu, F., Brandt, A., Gerdts, G., 2022. Human footprints at hadal depths: interlayer and intralayer comparison of sediment cores from the Kuril Kamchatka trench. Sci. Total Environ. 838, 156035 https://doi.org/10.1016/j.scitotenv.2022.156035.

Ådlandsvik, B., 2022. Lagrangian Advection and Diffusion Model (LADiM). https://github.com/bjornaa/ladim1.

Al-Azzawi, M.S.M., Kefer, S., Weißer, J., Reichel, J., Schwaller, C., Glas, K., Knoop, O., Drewes, J.E., 2020. Validation of sample preparation methods for microplastic analysis in wastewater matrices—reproducibility and standardization. Water 12, 2445. https://doi.org/10.3390/w12092445.

Allen, S., Allen, D., Moss, K., Le Roux, G., Phoenix, V.R., Sonke, J.E., 2020. Examination of the ocean as a source for atmospheric microplastics. PLoS One 15, e0232746. https://doi.org/10.1371/journal.pone.0232746.

AMAP, 2021. AMAP Litter and Microplastics Monitoring Guidelines. Version 1.0. Arctic Monitoring and Assessment Programme (AMAP), Tromsø, Norway, 257 pp.

Andrady, A.L., 2011. Microplastics in the marine environment. Mar. Pollut. Bull. 62, 1596–1605. https://doi.org/10.1016/j.marpolbul.2011.05.030.

Arthur, C., Baker, J., Bamford, H., 2009. Proceedings of the International Research Workshop on the Occurrence, Effects, and Fate of Microplastic Marine Debris, September 9–11, 2008. NOAA Technical Memorandum NOS-OR&R-30.

Bergmann, M., Wirzberger, V., Krumpen, T., Lorenz, C., Primpke, S., Tekman, M.B., Gerdts, G., 2017. High quantities of microplastic in Arctic deep-sea sediments from the HAUSGARTEN observatory. Environ. Sci. Technol. 51, 11000–11010. https://doi.org/10.1021/acs.est.7b03331.

Bergmann, M., Mützel, S., Primpke, S., Tekman, M.B., Trachsel, J., Gerdts, G., 2019. White and wonderful? Microplastics prevail in snow from the Alps to the Arctic. Sci. Adv. 5, eaax1157.

Bergmann, M., Collard, F., Fabres, J., Gabrielsen, G.W., Provencher, J.F., Rochman, C.M., van Sebille, E., Tekman, M.B., 2022. Plastic pollution in the Arctic. Nature Reviews Earth & Environment 3, 323–337. https://doi.org/10.1038/s43017-022-00279-8.

Choy, C.A., Robison, B.H., Gagne, T.O., Erwin, B., Firl, E., Halden, R.U., Hamilton, J.A., Katija, K., Lisin, S.E., Rolsky, C., Van Houtan, K.S., 2019. The vertical distribution and biological transport of marine microplastics across the epipelagic and mesopelagic water column. Sci. Rep. 9, 7843. https://doi.org/10.1038/s41598-019-44117-2.

Cole, M., Lindeque, P., Fileman, E., Halsband, C., Goodhead, R., Moger, J., Galloway, T. S., 2013. Microplastic ingestion by zooplankton. Environ. Sci. Technol. 47, 6646–6655. https://doi.org/10.1021/es400663f.

Courtene-Jones, W., van Gennip, S., Penicaud, J., Penn, E., Thompson, R.C., 2022. Synthetic microplastic abundance and composition along a longitudinal gradient traversing the subtropical gyre in the North Atlantic Ocean. Mar. Pollut. Bull. 185, 114371 https://doi.org/10.1016/j.marpolbul.2022.114371.

Cózar, A., Echevarria, F., Gonzalez-Gordillo, J.I., Irigoien, X., Ubeda, B., Hernandez-Leon, S., Palma, A.T., Navarro, S., Garcia-de-Lomas, J., Ruiz, A., Fernandez-de-Puelles, M.L., Duarte, C.M., 2014. Plastic debris in the open ocean. Proc. Natl. Acad. Sci. USA 111, 10239–10244. https://doi.org/10.1073/pnas.1314705111.

Cózar, A., Martí, E., Duarte, C.M., García-de-Lomas, J., Sebille, E.V., Ballatore, T.J., Eguíluz, V.M., González-Gordillo, J.I., Pedrotti, M.L., Echevarría, F., Troublè, R., Irigoien, X., 2017. The Arctic Ocean as a dead end for floating plastics in the North Atlantic branch of the Thermohaline Circulation. Sci. Adv. 3, e1600582.

D'Angelo, A., Trenholm, N., Loose, B., Glastra, L., Strock, J., Kim, J., 2023. Microplastics distribution within western Arctic seawater and sea ice. Toxics 11. https://doi.org/10.3390/toxics11090792.

Enders, K., Lenz, R., Stedmon, C.A., Nielsen, T.G., 2015. Abundance, size and polymer composition of marine microplastics >/=10mum in the Atlantic Ocean and their modelled vertical distribution. Mar. Pollut. Bull. 100, 70–81. https://doi.org/10.1016/j.marpolbul.2015.09.027.

Eriksen, M., Lebreton, L.C., Carson, H.S., Thiel, M., Moore, C.J., Borerro, J.C., Galgani, F., Ryan, P.G., Reisser, J., 2014. Plastic pollution in the World's oceans: more than 5 trillion plastic pieces weighing over 250,000 tons afloat at sea. PLoS One 9, e111913. https://doi.org/10.1371/journal.pone.0111913.

Gossmann, I., Herzke, D., Held, A., Schulz, J., Nikiforov, V., Georgi, C., Evangeliou, N., Eckhardt, S., Gerdts, G., Wurl, O., Scholz-Bottcher, B.M., 2023. Occurrence and backtracking of microplastic mass loads including tire wear particles in northern Atlantic air. Nat. Commun. 14, 3707. https://doi.org/10.1038/s41467-023-39340-5.

Gunaalan, K., Almeda, R., Lorenz, C., Vianello, A., Iordachescu, L., Papacharalampos, K., Rohde Kiaer, C.M., Vollertsen, J., Nielsen, T.G., 2023a. Abundance and distribution of microplastics in surface waters of the Kattegat/ Skagerrak (Denmark). Environ. Pollut. 318, 120853 https://doi.org/10.1016/j.envpol.2022.120853.

Gunaalan, K., Nielsen, T.G., Rodriguez Torres, R., Lorenz, C., Vianello, A., Andersen, C. A., Vollertsen, J., Almeda, R., 2023b. Is zooplankton an entry point of microplastics into the marine food web? Environ. Sci. Technol. 57, 11643–11655. https://doi.org/10.1021/acs.est.3c02575.

Gunaalan, K., Almeda, R., Vianello, A., Lorenz, C., Iordachescu, L., Papacharalampos, K., Nielsen, T.G., Vollertsen, J., 2024. Does water column stratification influence the vertical distribution of microplastics? Environ. Pollut. 340, 122865 https://doi.org/10.1016/j.envpol.2023.122865.

Haller, G., 2015. Lagrangian coherent structures. Annu. Rev. Fluid Mech. 47, 137–162. https://doi.org/10.1146/annurev-fluid-010313-141322.

Hanninen, J., Weckstrom, M., Pawlowska, J., Szymanska, N., Uurasjarvi, E., Zajaczkowski, M., Hartikainen, S., Vuorinen, I., 2021. Plastic debris composition and concentration in the Arctic Ocean, the North Sea and the Baltic Sea. Mar. Pollut. Bull. 165, 112150 https://doi.org/10.1016/j.marpolbul.2021.112150.

Huserbraten, M.B.O., Hattermann, T., Broms, C., Albretsen, J., 2022. Trans-polar drift-pathways of riverine European microplastic. Sci. Rep. 12, 3016. https://doi.org/10.1038/s41598-022-07080-z.

Isachsen, P.E., 2015. Baroclinic instability and the mesoscale eddy field around the Lofoten Basin. J. Geophys. Res. Oceans 120, 2884–2903. https://doi.org/10.1002/2014jc010448.

Kanhai, D.K., Gardfeldt, K., Lyashevska, O., Hassellov, M., Thompson, R.C., O'Connor, I., 2018. Microplastics in sub-surface waters of the Arctic Central Basin. Mar. Pollut. Bull. 130, 8–18. https://doi.org/10.1016/j.marpolbul.2018.03.011.
Karcher, M., Smith, J.N., Kauker, F., Gerdes, R., Smethie, W.M., 2012. Recent changes in Arctic Ocean circulation revealed by iodine-129 observations and modeling. J. Geophys. Res. Oceans 117. https://doi.org/10.1029/2011jc007513.
Kristiansen, T., Aas, E., 2015. Water type quantification in the Skagerrak, the Kattegat and off the Jutland west coast. Oceanologia 57, 177–195. https://doi.org/10.1016/j.oceano.2014.11.002.
Kroon, F., Motti, C., Talbot, S., Sobral, P., Puotinen, M., 2018. A workflow for improving estimates of microplastic contamination in marine waters: a case study from North-Western Australia. Environ. Pollut. 238, 26–38. https://doi.org/10.1016/j.envpol.2018.03.010.
Kvale, K., Prowe, A.E.F., Chien, C.T., Landolfi, A., Oschlies, A., 2020a. The global biological microplastic particle sink. Sci. Rep. 10 https://doi.org/10.1038/s41598-020-72898-4.
Kvale, K.F., Friederike Prowe, A.E., Oschlies, A., 2020b. A critical examination of the role of marine snow and zooplankton fecal pellets in removing ocean surface microplastic. Front. Mar. Sci. 6, 808. https://doi.org/10.3389/fmars.2019.00808.
Legendre, P., Gallagher, E.D., 2001. Ecologically meaningful transformations for ordination of species data. Oecologia 129, 271–280. https://doi.org/10.1007/s004420100716.
Leistenschneider, C., Burkhardt-Holm, P., Mani, T., Primpke, S., Taubner, H., Gerdts, G., 2021. Microplastics in the Weddell Sea (Antarctica): a forensic approach for discrimination between environmental and vessel-induced microplastics. Environ. Sci. Technol. 55, 15900–15911. https://doi.org/10.1021/acs.est.1c05207.
Leistenschneider, C., Wu, F., Primpke, S., Gerdts, G., Burkhardt-Holm, P., 2024. Unveiling high concentrations of small microplastics (11-500 μm) in surface water samples from the southern Weddell Sea off Antarctica. Sci. Total Environ. 172124 https://doi.org/10.1016/j.scitotenv.2024.172124.
Li, J., Shan, E., Zhao, J., Teng, J., Wang, Q., 2023. The factors influencing the vertical transport of microplastics in marine environment: a review. Sci. Total Environ. 870, 161893 https://doi.org/10.1016/j.scitotenv.2023.161893.
Lien, V.S., Gusdal, Y., Albretsen, J., Melsom, A., Vikebø, F., 2013. Evaluation of a Nordic Seas 4 km numerical ocean model hindcast archive (SVIM), 1960-2011. Fisken Havet 1–82.
Lien, V.S., Gusdal, Y., Vikebø, F.B., 2014. Along-shelf hydrographic anomalies in the Nordic seas (1960–2011): locally generated or advective signals? Ocean Dyn. 64, 1047–1059. https://doi.org/10.1007/s10236-014-0736-3.
Liu, M., Lu, S., Song, Y., Lei, L., Hu, J., Lv, W., Zhou, W., Cao, C., Shi, H., Yang, X., He, D., 2018. Microplastic and mesoplastic pollution in farmland soils in suburbs of Shanghai, China. Environ. Pollut. 242, 855–862. https://doi.org/10.1016/j.envpol.2018.07.051.
Liu, Y., Lorenz, C., Vianello, A., Syberg, K., Nielsen, A.H., Nielsen, T.G., Vollertsen, J., 2023. Exploration of occurrence and sources of microplastics (>10 mum) in Danish marine waters. Sci. Total Environ. 865, 161255 https://doi.org/10.1016/j.scitotenv.2022.161255.
Lorenz, C., Roscher, L., Meyer, M.S., Hildebrandt, L., Prume, J., Loder, M.G.J., Primpke, S., Gerdts, G., 2019. Spatial distribution of microplastics in sediments and surface waters of the southern North Sea. Environ. Pollut. 252, 1719–1729. https://doi.org/10.1016/j.envpol.2019.06.093.
Lusher, A.L., McHugh, M., Thompson, R.C., 2013. Occurrence of microplastics in the gastrointestinal tract of pelagic and demersal fish from the English Channel. Mar. Pollut. Bull. 67, 94–99. https://doi.org/10.1016/j.marpolbul.2012.11.028.
Lusher, A.L., Tirelli, V., O'Connor, I., Officer, R., 2015. Microplastics in Arctic polar waters: the first reported values of particles in surface and sub-surface samples. Sci. Rep. 5, 14947. https://doi.org/10.1038/srep14947.
Maes, T., Van der Meulen, M.D., Devriese, L.I., Leslie, H.A., Huvet, A., Frère, L., Robbens, J., Vethaak, A.D., 2017. Microplastics baseline surveys at the water surface and in sediments of the north-east Atlantic. Front. Mar. Sci. 4 https://doi.org/10.3389/fmars.2017.00135.
Mani, T., Primpke, S., Lorenz, C., Gerdts, G., Burkhardt-Holm, P., 2019. Microplastic pollution in benthic midstream sediments of the Rhine River. Environ. Sci. Technol. 53, 6053–6062. https://doi.org/10.1021/acs.est.9b01363.
Mork, K.A., Blindheim, J., 2000. Variations in the Atlantic inflow to the Nordic seas, 1955–1996. Deep-Sea Res. I Oceanogr. Res. Pap. 47, 1035–1057. https://doi.org/10.1016/S0967-0637(99)00091-6.
Mrokowska, M.M., 2020. Influence of pycnocline on settling behaviour of non-spherical particle and wake evolution. Sci. Rep. 10, 20595. https://doi.org/10.1038/s41598-020-77682-y.
Mu, J., Zhang, S., Qu, L., Jin, F., Fang, C., Ma, X., Zhang, W., Wang, J., 2019. Microplastics abundance and characteristics in surface waters from the Northwest Pacific, the Bering Sea, and the Chukchi Sea. Mar. Pollut. Bull. 143, 58–65. https://doi.org/10.1016/j.marpolbul.2019.04.023.
Nel, A.E., Mädler, L., Velegol, D., Xia, T., Hoek, E.M.V., Somasundaran, P., Klaessig, F., Castranova, V., Thompson, M., 2009. Understanding biophysicochemical interactions at the nano–bio interface. Nat. Mater. 8, 543–557. https://doi.org/10.1038/nmat2442.
O'Brien, S., Rauert, C., Ribeiro, F., Okoffo, E.D., Burrows, S.D., O'Brien, J.W., Wang, X., Wright, S.L., Thomas, K.V., 2023. There's something in the air: a review of sources, prevalence and behaviour of microplastics in the atmosphere. Sci. Total Environ. 874, 162193 https://doi.org/10.1016/j.scitotenv.2023.162193.
Peeken, I., Primpke, S., Beyer, B., Gutermann, J., Katlein, C., Krumpen, T., Bergmann, M., Hehemann, L., Gerdts, G., 2018. Arctic sea ice is an important temporal sink and means of transport for microplastic. Nat. Commun. 9, 1505. https://doi.org/10.1038/s41467-018-03825-5.
PlasticsEuope, 2022. Plastics - The Facts 2022. https://plasticseurope.org/knowledge-hub/plastics-the-facts-2022/.
PlasticsEurope, 2023. Plastics-The Fast Facts 2023. https://plasticseurope.org/knowledge-hub/plastics-the-fast-facts-2023/.
Primpke, S., Dias, A., Gerdts, G., 2019. Automated identification and quantification of microfibres and microplastics. Anal. Methods 11, 2138–2147. https://doi.org/10.1039/c9ay00126c.
Primpke, S., Lorenz, C., Rascher-Friesenhausen, R., Gerdts, G., 2017. An automated approach for microplastics analysis using focal plane array (FPA) FTIR microscopy and image analysis. Anal. Methods 9, 1499–1511. https://doi.org/10.1039/c6ay02476a.
Primpke, S., Wirth, M., Lorenz, C., Gerdts, G., 2018. Reference database design for the automated analysis of microplastic samples based on Fourier transform infrared (FTIR) spectroscopy. Anal. Bioanal. Chem. 410, 5131–5141. https://doi.org/10.1007/s00216-018-1156-x.
Primpke, S., Fischer, M., Lorenz, C., Gerdts, G., Scholz-Böttcher, B.M., 2020. Comparison of pyrolysis gas chromatography/mass spectrometry and hyperspectral FTIR imaging spectroscopy for the analysis of microplastics. Anal. Bioanal. Chem. 412, 8283–8298. https://doi.org/10.1007/s00216-020-02979-w.
Quinn, B., Murphy, F., Ewins, C., 2017. Validation of density separation for the rapid recovery of microplastics from sediment. Anal. Methods 9, 1491–1498. https://doi.org/10.1039/c6ay02542k.
Rao, C.R., 1995. A review of canonical coordinates and an alternative to correspondence analysis using Hellinger distance. Quest 19.
Rist, S., Vianello, A., Winding, M.H.S., Nielsen, T.G., Almeda, R., Torres, R.R., Vollertsen, J., 2020. Quantification of plankton-sized microplastics in a productive coastal Arctic marine ecosystem. Environ. Pollut. 266, 115248 https://doi.org/10.1016/j.envpol.2020.115248.
Roscher, L., Fehres, A., Reisel, L., Halbach, M., Scholz-Bottcher, B., Gerriets, M., Badewien, T.H., Shiravani, G., Wurpts, A., Primpke, S., Gerdts, G., 2021. Microplastic pollution in the Weser estuary and the German North Sea. Environ. Pollut. 288, 117681 https://doi.org/10.1016/j.envpol.2021.117681.
Roscher, L., Halbach, M., Nguyen, M.T., Hebeler, M., Luschtinetz, F., Scholz-Bottcher, B. M., Primpke, S., Gerdts, G., 2022. Microplastics in two German wastewater treatment plants: year-long effluent analysis with FTIR and Py-GC/MS. Sci. Total Environ. 817, 152619 https://doi.org/10.1016/j.scitotenv.2021.152619.
Ross, P.S., Chastain, S., Vassilenko, E., Etemadifar, A., Zimmermann, S., Quesnel, S.A., Eert, J., Solomon, E., Patankar, S., Posacka, A.M., Williams, B., 2021. Pervasive distribution of polyester fibres in the Arctic Ocean is driven by Atlantic inputs. Nat. Commun. 12, 106. https://doi.org/10.1038/s41467-020-20347-1.
Shchepetkin, A.F., McWilliams, J.C., 2005. The regional oceanic modeling system (ROMS): a split-explicit, free-surface, topography-following-coordinate oceanic model. Ocean Model 9, 347–404. https://doi.org/10.1016/j.ocemod.2004.08.002.
Simon, M., van Alst, N., Vollertsen, J., 2018. Quantification of microplastic mass and removal rates at wastewater treatment plants applying Focal Plane Array (FPA)-based Fourier Transform Infrared (FT-IR) imaging. Water Res. 142, 1–9. https://doi.org/10.1016/j.watres.2018.05.019.
Skagseth, Ø., Drinkwater, K.F., Terrile, E., 2011. Wind- and buoyancy-induced transport of the Norwegian Coastal Current in the Barents Sea. J. Geophys. Res. 116 https://doi.org/10.1029/2011jc006996.
Sokal, R.R., Rohlf, F.J., 1995. Biometry: The Principles and Practice of Statistics in Biological Research, third ed. Freeman, W.H., New York, USA.
Song, Y.K., Hong, S.H., Jang, M., Kang, J.H., Kwon, O.Y., Han, G.M., Shim, W.J., 2014. Large accumulation of micro-sized synthetic polymer particles in the sea surface microlayer. Environ. Sci. Technol. 48, 9014–9021. https://doi.org/10.1021/es501757s.
Suaria, G., Perold, V., Lee, J.R., Lebouard, F., Aliani, S., Ryan, P.G., 2020. Floating macro- and microplastics around the Southern Ocean: results from the Antarctic Circumnavigation Expedition. Environ. Int. 136, 105494 https://doi.org/10.1016/j.envint.2020.105494.
Sun, X., Li, Q., Zhu, M., Liang, J., Zheng, S., Zhao, Y., 2017. Ingestion of microplastics by natural zooplankton groups in the northern South China Sea. Mar. Pollut. Bull. 115, 217–224. https://doi.org/10.1016/j.marpolbul.2016.12.004.
Tanaka, K., Takada, H., 2016. Microplastic fragments and microbeads in digestive tracts of planktivorous fish from urban coastal waters. Sci. Rep. 6, 34351. https://doi.org/10.1038/srep34351.
Teichert, S., Loder, M.G.J., Pyko, I., Mordek, M., Schulbert, C., Wisshak, M., Laforsch, C., 2021. Microplastic contamination of the drilling bivalve Hiatella arctica in Arctic rhodolith beds. Sci. Rep. 11, 14574. https://doi.org/10.1038/s41598-021-93668-w.
Tekman, M.B., Wekerle, C., Lorenz, C., Primpke, S., Hasemann, C., Gerdts, G., Bergmann, M., 2020. Tying up loose ends of microplastic pollution in the Arctic: distribution from the sea surface through the water column to deep-sea sediments at the HAUSGARTEN observatory. Environ. Sci. Technol. 54, 4079–4090. https://doi.org/10.1021/acs.est.9b06981.
Thompson, R.C., Olsen, Y., Mitchell, R.P., Davis, A., Rowland, S.J., John, A.W., McGonigle, D., Russell, A.E., 2004. Lost at sea: where is all the plastic? Science 304, 838. https://doi.org/10.1126/science.1094559.
Uurasjarvi, E., Paakkonen, M., Setala, O., Koistinen, A., Lehtiniemi, M., 2021. Microplastics accumulate to thin layers in the stratified Baltic Sea. Environ. Pollut. 268, 115700 https://doi.org/10.1016/j.envpol.2020.115700.
Vroom, R.J.E., Koelmans, A.A., Besseling, E., Halsband, C., 2017. Aging of microplastics promotes their ingestion by marine zooplankton. Environ. Pollut. 231, 987–996. https://doi.org/10.1016/j.envpol.2017.08.088.
Wang, Z., Zhang, Y., Kang, S., Yang, L., Shi, H., Tripathee, L., Gao, T., 2021. Research progresses of microplastic pollution in freshwater systems. Sci. Total Environ. 795, 148888 https://doi.org/10.1016/j.scitotenv.2021.148888.

Wekerle, C., Wang, Q., Danilov, S., Schourup-Kristensen, V., von Appen, W.-J., Jung, T., 2017. Atlantic water in the Nordic Seas: locally eddy-permitting ocean simulation in a global setup. J. Geophys. Res. Oceans 122, 914–940. https://doi.org/10.1002/2016jc012121.

Winther, N.G., Johannessen, J.A., 2006. North Sea circulation: Atlantic inflow and its destination. J. Geophys. Res. 111 https://doi.org/10.1029/2005jc003310.

Witzig, C.S., Foldi, C., Worle, K., Habermehl, P., Pittroff, M., Muller, Y.K., Lauschke, T., Fiener, P., Dierkes, G., Freier, K.P., Zumbulte, N., 2020. When good intentions go bad-false positive microplastic detection caused by disposable gloves. Environ. Sci. Technol. 54, 12164–12172. https://doi.org/10.1021/acs.est.0c03742.

Zhao, J., Ran, W., Teng, J., Liu, Y., Liu, H., Yin, X., Cao, R., Wang, Q., 2018. Microplastic pollution in sediments from the Bohai Sea and the Yellow Sea, China. Sci. Total Environ. 640-641, 637–645. https://doi.org/10.1016/j.scitotenv.2018.05.346.

Zhao, S., Zettler, E.R., Bos, R.P., Lin, P., Amaral-Zettler, L.A., Mincer, T.J., 2022. Large quantities of small microplastics permeate the surface ocean to abyssal depths in the South Atlantic Gyre. Glob. Chang. Biol. 28, 2991–3006. https://doi.org/10.1111/gcb.16089.

Zobkov, M.B., Esiukova, E.E., Zyubin, A.Y., Samusev, I.G., 2019. Microplastic content variation in water column: the observations employing a novel sampling tool in stratified Baltic Sea. Mar. Pollut. Bull. 138, 193–205. https://doi.org/10.1016/j.marpolbul.2018.11.047.